Biomass and Bioenergy 193 (2025) 107560

Contents lists available at ScienceDirect

Biomass and Bioenergy

journal homepage: www.elsevier.com/locate/biombioe

Oxidative electrochemical depolymerization of lignin using highly active self-standing electrocatalysts prepared by electrospinning of lignin

M. García-Rollán, M. Toscano-de los Riscos, R. Ruiz-Rosas *, J.M. Rosas, J. Rodríguez-Mirasol, T. Cordero

Universidad de Málaga, Andalucía Tech., Departamento de Ingeniería Química, Campus de Teatinos s/n, 29010, Málaga, Spain

ARTICLE INFO

Keywords:
Lignin
Electrocatalysts
Carbon nanofibers
Depolymerization
Electrooxidation
Aromatic monomers

ABSTRACT

Electrooxidative depolymerization of lignin enables obtaining renewable value-added chemicals under soft operation conditions. However, current nickel foam electrodes do not fully utilize their active phase. In this study, non-woven mats consisting of metal-containing carbon nanofibers were prepared by electrospinning of lignin and Ni, Co and/or Pd solutions. These mats, without further processing and additives, were tested as self-standing electrodes in the electrooxidative depolymerization of alkaline kraft lignin solution using a filter press electrolyzer at room temperature. The fibrillar electrocatalyst containing 10 % wt of Ni (CFNi10) showed the most promising results, producing i) up to 77 % of oxygen-rich depolymerized lignin solid, ii) a water-soluble fraction yield up to 19.8 % wt iii) total vanillin yield of 1.1 % wt, using specific charges as low as 250 C/g_{lignin}, outperforming the commercial nickel foam electrode, and iv) full reusability. Consequently, the activity of the process is improved, while the amount of nickel deployed on the electrochemical cell is notably decreased from 30 down to 0.3 mg/cm^2. The results of the present paper also demonstrate that lignin electrochemical depolymerization needs to be promoted by reactive oxygen species and/or in-situ generation of hydrogen peroxide.

1. Introduction

Lignocellulosic biomass is considered as the most promising renewable source of energy and added-value products. The sustainability of lignocellulosic-based industrial processes is highly reliant on full valorization of all biopolymers present in lignocellulosic biomass, i.e. cellulose, hemicellulose and lignin [1]. Lignin is a three-dimensional and heterogeneous macromolecule that is mainly composed of aromatic rings, making it the largest biobased feedstock for sustainable production of aromatic chemicals. Lignin polymeric structure enables direct uses in obtaining biobased materials as cement additives, polymeric blends or phenolic resins, among others [2]. In addition, value-added chemicals can be obtained from lignin through depolymerization [3,4], while the high aromatic carbon content also allows obtaining advanced carbon materials such as carbon fibers, carbon molecular sieves, hierarchical porous carbons or activated carbons [5,6].

Lignin depolymerization is carried out through thermochemical, reductive and oxidative methods and the distribution of aromatic products vary according to the operating conditions. Generally, these depolymerization methods requires either high pressure and/or high temperature, involves the use of toxic chemicals, noble metals as catalysts and often are non-selective, producing a large collection of products and leading to the development of greener depolymerization processes [7,8]. Novel sustainable strategies are needed to increase selectivity and decrease the requirement of critical elements.

Electrochemical treatment of lignin is a method with high potential for lignin depolymerization that is fully integrated with the green chemistry principles. Compared to traditional oxidative depolymerization of lignin, the electrochemical process stands out for its mild reaction conditions, i.e. atmospheric pressure and room temperature [9]. In a similar way to conventional methods, the electrochemical cleavage of lignin can be achieved via reductive treatment at cathode, oxidative treatment at the anode and even through the combination of both processes. Anodic oxidation is the most investigated and reported treatment in the literature for lignin conversion [10–18], but some literature can be also found about reductive and combined treatments [18–21]. In the

* Corresponding author. Universidad de Málaga, Andalucía Tech., Departamento de Ingeniería Química, Escuela de Ingenierías Industriales, Campus de Teatinos s/n, 29010, Málaga, Spain.
E-mail address: ramiro@uma.es (R. Ruiz-Rosas).

https://doi.org/10.1016/j.biombioe.2024.107560
Received 4 September 2024; Received in revised form 20 November 2024; Accepted 15 December 2024
Available online 22 December 2024

latter approach, three strategies can be followed, i.e., direct, indirect and electrical-chemical combination reactions [10,11]. In direct electrooxidation, the electrode itself acts as a heterogeneous electrocatalyst, producing the so-called lignin or lignin model compounds oxidation on it [22,23]. For this purpose, transition metals such as nickel or cobalt, noble metals as Pd, Ru or Pb/PbO_2 are usually used [24–26]. As for indirect electrooxidation, a homogeneous electrocatalyst or a redox mediator accepts the electrons from the lignin molecules. The reduced mediator is regenerated on the electrode surface after transferring the electrons (i.e. it is oxidized). The most used homogeneous electrocatalysts are polyoxometalates, laccases or TEMPO (2,2,6,6-tetramethylpiperidine-N-oxyl), with transition-metal complexes gaining more attention recently [27,28]. Finally, in the electrical-chemical combination reaction, lignin can be oxidized both at the anode and within the solution by the effect of reactive oxygen species (such as radical oxygen species or H_2O_2) that can be produced at the cathode and/or at the anode [26]. The electrocatalytic oxidation of lignin generates the formation of aromatic monomers derived from the monomeric units found on the starting lignin, along with a decrease in the average molecular weight distribution [10]. Usually, a harsher applied voltage or intensity current during the treatment leads to stronger depolymerization degree of lignin and higher monomeric yield. However, excessive oxidation can not only lead to monomeric decomposition or even full mineralization of lignin, but under these extreme conditions in aqueous medium, it can also trigger other competing reactions such as the oxygen evolution reaction (OER) involving the oxidation of water to produce molecular oxygen, protons and electrons detracting from the efficiency and selectivity of lignin oxidation by diverting the electrochemical resources needed for the desired reaction [29].

The performance of the electrochemical cells is dominated by the efficiency of the electrodes, which must have high electrical conductivity and a large electroactive surface area, in addition to high chemical and mechanical resistances [30]. In this sense, nickel foams and graphite felts and papers, which are composed by carbon fibers, fulfill these requirements. Therefore, they currently are the electrode of choice for a large collection of commercial electrochemical applications. However, nickel is regarded as a critical mineral [31], whereas carbon fibers are mostly prepared from polyacrylonitrile, which has a non-renewable origin, and the carbonized fibers are prepared by wet or melt spinning, showing sizes well over the micron scale. The limitation of the current methods for the preparation of carbon fibers can be overcome by electrospinning, a top-down and scalable technique that allows the production of nanofibers, with a high surface-to-volume ratio, by subjecting a polymeric solution of certain viscosity and electrical conductivity to an electric field [32]. Such carbon fibers have been identified as promising electrocatalysts for different applications, such as energy storage or electro-adsorption [33,34]. In addition, lignin is an ideal raw material for the preparation of carbon fibers due to the high carbon content and aromatization degree [5]. Indeed, lignin can be processed into carbon fibers using electrospinning [5] and it has been successfully used for the preparation of flexible porous carbon mats with high electrical conductivity and porosity [35], showing outstanding performance as electrodes of supercapacitors [36], redox flow batteries [37] or sodium metal batteries [38]. Moreover, fibrillar carbon catalysts and electrocatalysts containing heteroatoms and metals can be easily obtained by dissolving small quantities of inorganic salts and/or acids in the lignin solution for electrospinning. Following this one-pot procedure, the preparation of P-containing acid catalysts, cobalt-containing porous carbon fiber catalysts and platinum containing electrocatalysts have been reported [39,40]. On the other hand, the main problems related to the electrooxidative depolymerization of lignin are strongly related to the low lignin conversion per unit of catalyst specie, the low stability of the catalysts at the reaction conditions and the associated high cost of catalyst preparation [41]. Several studies have tackled these challenges by generating reactive oxygen species, such as H_2O_2, through the use of anodes made from noble metals like Ru, Ir, or Pt, as well as carbon-based materials such as graphite felt or glassy carbon [26, 42–47]. These anodes, when employed in different electrolytes, have shown effectiveness in promoting lignin depolymerization. However, to our knowledge, electrodes made of electrospun carbon nanofibers loaded with metals remain unexplored as electrocatalysts for lignin electrooxidation. Herein, the authors present, for the first time, the use of carbon fibers prepared by electrospinning of lignin for the electrooxidative depolymerization of lignin. This dual valorization of this residue, transforming it into industrially interesting carbon fiber-based electrocatalysts and producing high-value compounds from its electrooxidation, represents a pioneering approach that could greatly improve not only the sustainability of the process, but also solving the problems mentioned above. Hence, metal loaded electrospun carbon fibers have shown high stability and activity as catalysts for different reactions owing to a well-dispersed and accessible active phase, high porosity and outstanding heat and electrical conductivity [35,40,48]. In addition, the use of lignin, a lignocellulosic residue, as a feedstock helps to circumvent the high costs typically associated with catalysts.

This work analyzes the electrooxidation of Kraft lignin using anodic electrodes derived also from lignin and prepared by electrospinning technique. The optimization of the preparation conditions of the lignin fibers and the metal-containing lignin fibers, as well as the performance of transition or noble metal-containing carbon fibers as electrocatalysts have been studied. Special attention has been paid to the yields toward different electrooxidation products, and also to characterize the composition of the liquid products and the solid fraction generated by the electrochemical oxidation of lignin.

2. Materials and methods

2.1. Chemicals

Indulin-AT (IND), a pine wood Kraft lignin, was produced by Westvaco Chemical Division. Organosolv lignin was supplied by American Science and Technology Corp (AST). Polyvinylpyrrolidone (PVP) (Mw = 1,300,000 g/mol), acetic acid (glacial, ≥ 99 %), Nafion® (5 % wt perfluorinated resin solution), nickel (II) acetate tetrahydrate (98 %), cobalt (II) acetate tetrahydrate (reagent grade, 98 %) and palladium (II) acetate (reagent grade, 98 %) were provided by Sigma-Aldrich. NaOH (98 %) was purchased from PanReac AppliChem. N_2 5.0 quality (purity of 99.999 %) was provided by Linde.

2.2. Catalysts synthesis

Lignin fibers were prepared by electrospinning technique using coaxial configuration as reported elsewhere [49,50]. In that way, a solution of AST-PVP with acetic acid as solvent flows through the inner injector, while additional acetic acid is pumped through the outer needle to avoid solidification of the Taylor cone. AST concentration was varied between 27 and 40 % wt, whereas PVP concentrations between 1 and 5 % wt were used. In a typical synthesis, 0.55 g of PVP and 5 g of AST were loaded into a 50 mL glass flask. Then, 12.3 mL of acetic acid was poured into the glass flask, which was stopped and kept under constant stirring at 200 rpm overnight. The resulting lignin-PVP solution was fed through the inner needle of the coaxial spinneret at 2 mL/h using a syringe pump (Cole Palmer®, Vernon Hills, Illinois). Acetic acid was added through the outer needle using a flow rate of 0.4 mL/h. The applied electrical potential difference between the needle and the collector electrodes, which were set at 20 cm of distance, was 26 kV.

Nickel-, cobalt- and palladium-containing lignin fibers were prepared by the addition of the corresponding acetate salt, i.e. $Ni(CH_3CO_2)_2{\cdot}4H_2O$, $Co(CH_3CO_2)_2{\cdot}4H_2O$ or $Pd(CH_3CO_2)_2$ to the initial solution, in order to obtain a metal content on the final carbon fiber of 10 % wt for Ni and 3 % wt for Ni, Co and Pd. In addition to monometallic-containing carbon fibers, bimetallic Ni-Co and Ni-Pd carbon-based fibrillar electrocatalysts were prepared using nominal

weight ratios of 1:4 and 1:3, respectively.

In order to avoid the softening and melting of the lignin fiber during the subsequent thermal treatment, an oxidative thermostabilization process was necessary due to the low glass transition temperature (Tg) of lignin. In this line, air oxidation is widely known and used method of stabilization due to its cost-effectiveness [51]. Thus, all the lignin fibers were oxidized in a programmable oven (J.P. SELECTA, s.a., Barcelona, Spain), being heated from 50 °C to 200 °C with a heating rate of 1.8 °C/h, similar to previously reported [52]. The stabilized samples were heat treated at 900 °C in a horizontal furnace (CARBOLITE GERO, Hope Valley, United Kingdom) with a N_2 flow of 150 mL STP/min using a heating rate of 10 °C/min, as previously reported [53]. The carbonized samples were cooled to room temperature keeping the N_2 flow. The resulting electrocatalysts consist of non-woven mats of carbon fibers containing different metals. In this way, 7 different electrocatalysts were obtained and labelled as CF followed by the metal and the amount of it they contain. CFNi10 was used for the specific case of carbon fiber with 10 % wt of Ni.

2.3. Characterization of the samples

The composition of IND and AST lignins were analyzed in terms of moisture (ASTM E−949), volatile matter (ASTM E−872) and ash (ASTM E−1755) contents, while fixed carbon was obtained by difference. Ultimate analysis was carried out in order to assess the chemical composition of lignin using a CNHS EA3000 (Eurovector), which measured the C, H, N and S concentration simultaneously, while the amount of O was calculated by difference. Gel permeation chromatography (GPC) analyses were performed on samples with a 1260 Infinity II LC System (Agilent) equipped with three 300 × 7.5 mm PLgel 3 μm MIXED-E columns in series and a refractive index detector. THF was used as eluent with a flow rate of 1 cm^3/min. The operating conditions were 14 Mpa of pressure and 42 °C of temperature in the columns. The injection was carried out using 20 μL of a 10 mg/cm^3 lignin solution in THF. Polystyrene samples with different molecular weight (ranging from 70,000–266 Da from Sigma Aldrich) were used as calibration standard and toluene was used as a flow marker. Differential scanning calorimetry (DSC) was performed on a METTLER TOLEDO differential scanning calorimeter equipment, DSC 1 model, with a 50 cm^3/min air flow. Prior to analysis, the AST was dried in an oven for 12 h at 60 °C. Then the sample was first heated from room temperature to 90 °C for 1 h, cooled to room temperature and heated again to 150 °C in order to determine the glass transition (Tg) of the sample.

The morphology and texture of the carbon fibers were studied by scanning electron microscopy (SEM) and transmission electron microscopy (TEM), respectively. SEM images were taken in a JSM 6490LV (JEOL) microscope working at 20 kV, whereas TEM ones were recorded in a Talos F200X (Thermo Fischer Scientific) microscope at 200 kV. The average size of the carbon fibers was estimated from SEM and TEM images, using imageJ program, after the analysis of more than 120 cases for each different fiber. Similarly, the average metal particle size in the carbon fibers was determined with 100–200 particles presented in the TEM images using the imageJ software. The X-ray diffraction (XRD) patterns of the carbon fibers were registered in an EMPYREAN diffractometer (PANalytical) equipment, with 45 kV over a 2θ range of 5-80 °, a CuKα1 (1.5406 Å) monochromatic radiation and 40 mA. The average crystal size was calculated using the Scherrer equation. The leaching of nickel onto the lignin solution was checked in the EAT unit of SCAI by Inductively Coupled Plasma Mass Spectrometry (ICP-MS) in a NEXION 300D (PerkinElmer) attached to a single quadrupole mass spectrometer detector and He gas collision cell.

The porosity of the carbon fibers was analyzed by N_2 adsorption-desorption at −196 °C and CO_2 adsorption at 0 °C, with a Micromeritics ASAP2020 equipment. All the samples were subjected to degasification for at least 8 h at 150 °C. The specific surface area (A_{BET}) was obtained from N_2 adsorption-desorption isotherm using the BET equation. In addition, micropore volume (V_s) were assessed with the α_s method. Moreover, the volume of mesopore (V_{mes}) was calculated as the difference between the adsorbed volume at relative pressure of 0.98 and Vs. In order to determine the narrow micropore volume (V_{DR}), the Dubinin-Radushkevich method was applied to the CO_2 adsorption. To calculate those mentioned textural parameters from the N_2 isotherms at −196 °C and CO_2 at 0 °C, the IUPAC recommendations have been followed [54]. With the objective of obtaining the pore size distribution, the 2D-NLDFT heterogeneous surface model combining both the N_2 and CO_2 adsorption isotherms was used [55]. The X-ray photoelectron spectroscopy (XPS) was used to analyze the surface chemistry of the carbon fibers. This analysis was carried out with a PHI 5000 VersaProbe II equipment working with a monochromatic Al Kα radiation source (1486.6 eV). The maximum of the C1s peak has been positioned to the XPS photoemission energy of the C-C and C=C bonds (284.5 eV) as the internal reference to correct the position of the other peaks. The bulk inorganic composition of all the samples was determined by X-Ray Fluorescence (XRF) analysis in an atomic fluorescence wavelength dispersive spectrometer THERMO ARL PERFORM'X equipment.

The electrochemical characterization of the electrocatalysts was carried out using a Biologic SP-200 potentiostat in a standard three electrode cell equipped with a Pt wire as counter electrode and a commercial Ag/AgCl/KCl 1 M electrode (HI5313, Hanna Instruments) as the reference one. The electrocatalysts were cut into rounded slices (Ø: 3 mm, specific weight of 2–3 mg/cm^2) with a puncher. The slices were fixed to the tip of glassy carbon rod (diameter of 3 mm) using 3 μl of Nafion® (5 % wt perfluorinated resin solution), and the resulting assembly was used as the working electrode. A 1 M NaOH aqueous solution was used as supporting electrolyte. N_2 was bubbled in the cell for 5 min before the analysis. The electrochemical properties of the electrocatalysts were studied by cyclic voltamperometry under a potential window of −0.5 to 0.8 V at 10 mV/s of scan rate. The electrochemical response of the electrocatalysts for IND lignin oxidation reaction was also evaluated under the same conditions by adding 5 g/L of lignin into the NaOH solution.

2.4. Electrooxidation experiments and product characterization

The electrooxidative depolymerization of lignin was carried out in a batch electrolyzer using an electrochemical filter-press cell. A scheme of the experimental setup is shown in Fig. S1. The electrolyte, which was always circulating in a close loop, was supplied to the filter-press cell by a Multifix peristaltic pump attached to a 100 mL tank. Either nitrogen or oxygen were bubbled in the tank to control the possible contribution of the electrochemical reduction of oxygen into hydrogen peroxide to the lignin depolymerization process. As for the electrode assembly, a 4 cm^2 square slice of the electrocatalyst mats were cut and attached to the current collector through a SS-304 mesh, which enhanced the contact by decreasing the ohmic drop between the collector and the electrodes. The metal-containing electrocatalysts were placed as positive electrode, whereas the metal-free carbon fibers served as negative electrode. Commercial nickel foam (1 mm thickness) and Toray carbon paper (0.37 mm thickness) were also used as positive and negative electrodes, respectively, for benchmarking purposes. In order to avoid short circuits in the system, the electrodes were physically separated using a Nylon membrane (0.45 μm, Millipore). In a typical run of electrooxidation reaction, 100 mL of a 1M NaOH solution with 25 g/L of IND lignin were added to the electrolyzer tank and pumped through the filter-press cell at a flow rate of 360 mL/min. Sample aliquots were extracted at different reaction times between 0 and 4 h to determine the concentration of the different products. The residual lignin and the corresponding liquid products were recovered and analyzed at the end of the run.

2.4.1. Direct electro-oxidation, electrical-chemical ROS-assisted and electrical-chemical H_2O_2-assisted lignin depolymerization experiments

Fig. S1B shows the batch electrolyzer configuration used for studying the direct electrooxidation of lignin. To ensure that the oxidation process only proceeded from the oxidative effect of the positive electrode, the solution was previously deoxygenated with a constant bubbling of N_2. The potential of the positive electrode was fixed in order to achieve a potential of 0.6 V vs the standard hydrogen electrode (SHE), i.e. the onset potential to enable the direct lignin electrooxidation process, by placing a calomel reference electrode (HI5412, Hanna Instruments) in the electrolyte tank.

The same configuration was used for the study of the assisted electrooxidation of lignin by radical oxygen species (ROS) Fig. S1C. For this purpose, the formation of ROS on the positive electrode was promoted by working under galvanostatic mode, setting the current intensity at values of 100, 200 and 400 mA, based on geometric current density values previously reported in the literature [56].

Finally, the electrooxidation of lignin through the combined formation of ROS at the anode and hydrogen peroxide produced by oxygen reduction at the cathode was also studied. The 10 % wt. nickel fibrillar electrocatalyst was set as anode and the metal-free carbon fibers as cathode as depicted in Fig. S1D. In this experiment, O_2 was bubbled at 50 ml/min STP in the electrolyte tank. The oxygen-saturated electrolyte solution containing the IND lignin at concentrations of 25 g/L or 100 g/L was forced to circulate from both sides of the cell, while the electrical current was set to 100 mA.

Using the last setup, the performance of commercial nickel foam and Toray paper electrodes was assessed for the sake of comparison. The reusability as electrocatalyst of the lignin-based carbonized mats was also evaluated in this configuration by cleansing the filter-press electrodes by pumping 100 mL of 1 M NaOH solution for 10 min and replacing the 100 g/L lignin solution in the tank with a fresh one before running a second test.

2.4.2. Reaction products analysis

The concentration of the monomers produced by the depolymerization of IND lignin during its electrooxidation was monitored by sampling at different time intervals following the protocol depicted in Scheme S1. Briefly, 1 mL of reaction liquid was taken from the lignin tank, acidified with concentrated HCl in order to remove the lignin, and extracted with ethyl acetate (EtAc), with a reaction liquid to EtAc ratio value of 10 (v:v), until the aqueous phase showed negligible amounts of lignin depolymerization products. The EtAc phase is diluted 1:100 in EtAc for the qualitative identification of the monomeric products, using a gas chromatograph coupled to a mass spectrometer Agilent 7000 D GC/MS Triple Quad (GC-MS), equipped with a 30 m DB-624 column. The chromatographic method started at 60 °C, with a final temperature of 240 °C and a heating rate of 8 °C/min and holding time of 20 min. Calibration curves in the 1–50 ppm range, using dodecane as external standard, were established for the determination of the concentration of the most abundant monomers.

The remaining lignin along with the organic compounds were precipitated from the solution by adding concentrated HCl for the determination of the solid and the corresponding total monomers and oligomers yields. The Total Organic Content (TOC) of the liquid phase was determined in a multi N/C 3100 + HT 1300 (Analytik Jena) using a 1:50 dilution in distilled water. The solid fraction was washed with distilled water to remove salts, dried at 60 °C overnight, weighted and submitted to different characterization analyses to evaluate the changes in composition and structure.

Finally, the lignin conversion and the selectivity and yield to the different oxidation products were calculated as follows:

$$\text{Conversion}\ (\%) = \frac{\text{Initial lignin (wt)-residual lignin (wt)}}{\text{Initial lignin (wt)}} \text{x } 100 \quad (1)$$

$$\text{Selectivity}\ (\%) = \frac{\text{Product}_i\ (\text{wt})}{\sum \text{Product}_i (\text{wt})} \text{x } 100 \quad (2)$$

$$\text{Product yield}\ (\%) = \frac{\text{Product}_i\ (\text{wt})}{\text{Initial lignin (wt)}} \text{ x } 100 \quad (3)$$

Where *initial* and *residual lignin* are the weight of the lignin at the beginning of the reaction and the weight of the solid remaining at the end of the reaction, respectively, while $Product_i$ is the weight of vanillin, guaiacol, acetovanillone or the rest of the identified and quantified monomers by GC-MS.

3. Results and discussion

3.1. Lignin characterization

The most relevant physicochemical properties of the AST and the IND lignins are compiled in Table 1. The elemental composition shows that both lignins have a similar carbon and hydrogen content. Their high carbon amount indicates their promising potential to prepare carbon materials with a high yield. In addition, the presence of nitrogen in AST lignin could make it a interesting raw material for the preparation of carbon fibers with nitrogen functionalities, which are known to improve wettability and electrical conductivity in carbon materials and generates catalytic active sites for electrochemical reactions [57]. In contrast, the high content of sulfur in the IND lignin disables any potential use as carbon precursor for the preparation of Pd, Ni and Co electrocatalyst, since sulfur poisons noble metal catalysts and it would form sulfides with transition metals during the carbonization of the metal-containing lignin fibers. Proximate analyses show lower amounts of impurities in the organosolv lignin, AST (i.e. ash content) compared to Kraft lignin, IND, due to the use of NaOH and Na_2S during the extraction of the latter.

The molecular weight and the polydispersity of the lignins have been studied by GPC. Table 1 collects the molecular weight (MW) and the polydispersity (PD) of the lignin and Fig. S2 represents the corresponding molecular weight distribution. Traditionally, the production of fibers by electrospinning requires the preparation of a solution with high enough viscosity to balance the surface tension of the solvent. For this reason, polymers used in electrospinning usually have a high molecular weight. However, AST lignin shows a molecular weight of 1611 mol/g and a polydispersity of 2.33 (Table 1), which makes it very difficult to produce a solution with the appropriate rheological properties for electrospinning.

Moreover, DSC Curve in Fig. S3 reveals glass transition temperature (T_g) of 60 °C and low melting point (T_m) for the AST lignin. To increase Tg and prevent softening during heat treatment process to produce the carbonization of the lignin fibers, an oxidative stabilization treatment at low heating rates prior the carbonization, which favors polymer cross-linking reactions, is required [51]. Further methods for minimizing the thermostabilization time of lignin fibers can be found in literature, such as spinning with small amounts of phosphoric acid [58], or adding a copolymer in the spinning solution [59]. The latter approach was chosen in this case by adding PVP to the electrospinning solution.

The preparation of AST lignin fibers by co-axial electrospinning was studied at different AST lignin (24–41 % wt) and PVP (1–5 % wt) concentrations. The best conditions to produce fibers were obtained with 27 % wt of AST lignin and a 9:1 lignin:PVP mass ratio. The corresponding SEM micrographs of the fibers obtained at the different experimental conditions can be found in Fig. S4A-G, confirming that, under these conditions, continuous lignin fibers with high aspect ratios and smooth surfaces are obtained even when the $NiAc_2{\cdot}4H_2O$ content is increased up to 5 % wt to the electrospinning solution, Fig. S4F, enabling the obtention of the metal-containing carbon fibers in just one preparation step.

Table 1
Physicochemical properties of raw lignins.

Sample	Ultimate analysis (% wt)					Ash (%wt)	XRF (% wt)		GPC	
	C	H	N	S	O		Na	Others	MW (g/mol)	PD
AST	64.9	6.7	2.5	0.3	25.6	<0.1	<0.1	<0.1	1611	2.3
IND	62.3	6.0	0.8	1.2	29.7	2.7	0.3	0.9	6549	9.9

3.2. Carbon fibers production and characterization

Electrospinning of PVP-lignin solutions produces flexible non-woven mats that can be easily shaped or cut into the desired geometry to be fit into the electrolyzer filter-press cell. However, these mats need to be carbonized in order to decompose the metal precursor, produce the metal nanoparticles that serve as catalytic sites and generate carbonized fibers with enhanced electrical conductivity. As stated before, the electrospun mats require pretreatment to increase the glass transition temperature before carbonization, avoiding partial fusing or melting of the fibers in the process. For this purpose, they are submitted to an air stabilization step [35].

Fig. 1 shows SEM images of the metal-free and metal-loaded carbon mats. The fibers have retained fibrillar morphology after carbonization, with no signs of total or partial melting during carbonization. Most fibers seem to show smooth surfaces and to be continuous, thus presenting a high aspect ratio. The average carbon fiber diameters, determined from SEM images, are also represented in Fig. 1G. The diameters are in the range of 0.8–0.9 μm, exception made of the fibers without metallic phase, which shows a larger size, and the CFNiPd sample. The smaller sizes obtained in metal-containing CFs are mostly explained by the solution conductivity, which needs to be compensated by increasing the lignin solution feed rate and the applied potential difference in electrospinning process. The obtained diameters are far below those obtained with other spinning techniques, such as melt or thermal spinning [60], being ten times smaller than the carbon fibers of gas diffusional layers used for supporting electrocatalysts, such as Toray's carbon fiber paper [61].

The thermostabilization, carbonization and overall treatments yields of different carbon fibers production are also summarized in Table 2. The air stabilization stage resulted in a significant loss of mass, which might be related to the evaporation of occluded acetic acid (≈30 % wt) and to the evolution of H_2O from condensation and dehydration reactions involved in the crosslinking process, which increases the Tg of the lignin fibers [52]. The relatively low yield observed in the CFs after the stabilization process, compared to those obtained by the stabilization of electrospun Alcell lignin fibers (61 vs 76–77 % wt) [53,58], is probably connected to the high sugar content of the AST lignin studied in this work (18 % wt of holocellulose content, measured according to ASTM D-1104).

Table 2
Thermostabilization, carbonization and overall treatments yields of the preparation of the carbon fibers.

Sample	Yield (% wt)		
	Stab.	Carb.	Overall
CF	61	43	26
CFNi3	72	41	30
CFNi10	73	40	29
CFCo	70	39	28
CFPd	68	50	34
CFNiCo	74	39	29
CFNiPd	69	46	32

The presence of metal in the polymeric fiber slightly increases the yield in the stabilization step, probably due to the formation of metal oxides and catalytic oxidation of lignin. A similar behavior has been recently observed during the air stabilization step of electrospun cobalt-loaded Alcell lignin fibers [40]. Carbonization yields are between 40 and 50 % wt, Table 2. The loss of volatile matter, the decomposition of surface oxygen groups and metal acetate salts and the carbothermal reduction of the resulting metal oxides take part during carbonization of metal-containing lignin fibers, with different extends depending on the nature of the involved metal [40].

The structure of the carbonized fibers has been studied by TEM, Fig. 2A-F. The lack of defects is a common feature of all the analyzed carbonized fibers. However, the distribution and sizes of metallic nanoparticles greatly depends on the nature of the metallic phase, as depicted by the average size values reported in Fig. 2G. The micrographs reveal that CFNi3 have discrete and large-sized nanoparticles, while CFPd micrographs show smaller and well distributed nanoparticles (average size of 7.3 nm vs 17.2 nm for the former sample), which suggests a greater sintering of Ni during carbonization. The size of nickel nanoparticles increases from 17.2 up to 19.4 nm with metal loading, as denoted by the formation of particles as large as 50 nm on the surface of CFNi10, Fig. 2D. Differently, Co is capable to be finely dispersed on the surface of the fiber, presenting the smallest nanoparticle sizes and a narrower particle size distribution than those of CFPd and CFNi3 counterparts (see inset on Fig. 2B). Similar trends are observed for the

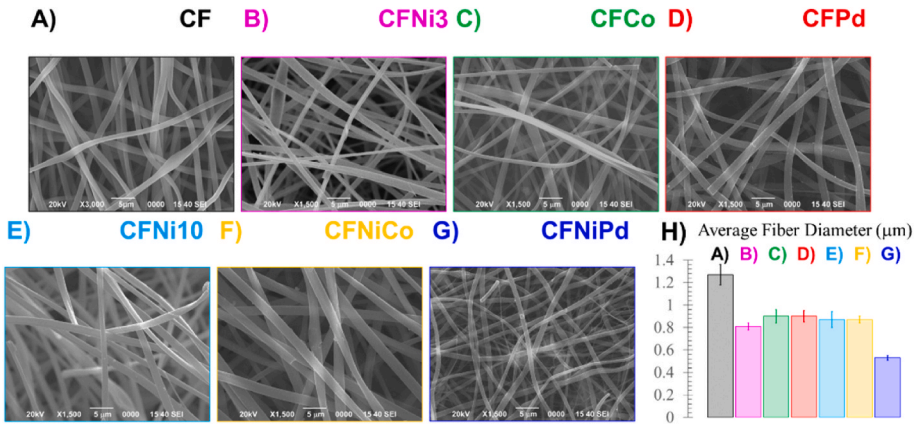

Fig. 1. SEM images of the different electrospun carbonized fiber & average fiber diameter of the carbon fibers.

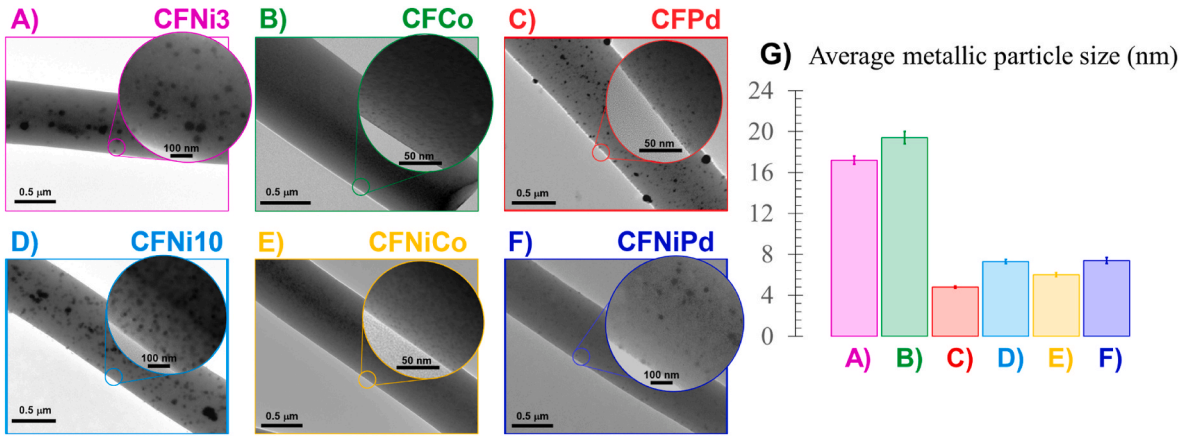

Fig. 2. TEM images of the electrospun metal-containing carbon fibers & average particle size of the metallic phase.

bimetallic electrocatalysts, where the addition of Ni to Co- and Pd-catalysts results in a small size increase, Table 2.

The crystalline dispersion of the active phase of the electrocatalysts have been also tracked by XRD. The diffraction patterns of the different carbon fibers (Fig. S5A) show as a shared feature a broad peak at 43°, corresponding to the (10) peak of graphite. The development of this peak is related to the lateral size of the graphene-like layers composing the CFs, a desirable feature that increases the electrical conductivity of the carbon fibers [35]. The presence of metals in the CFs provides an additional positive outcome, since the (10) peak gets narrower and better defined. Only the peaks corresponding to crystalline metallic nickel (at 44.5 and 51.9°) in the CFNi3 and CFNi10 samples are observed. From these results, average crystal sizes of 18.2 and 23.7 nm can be derived for these two samples, respectively, which seem to agree well with TEM results. No other signals have been detected for the rest of the samples, ruling out the presence of crystal sizes larger than 5 nm (i.e. the lower detection limit of the XRD device).

The porosity and apparent surface area are key parameters for the performance of electrocatalysts. Table 3 summarizes the main textural parameters derived from N_2 adsorption-desorption isotherm and CO_2 adsorption isotherm obtained at −196 °C and 0 °C, respectively. The results show that microporosity is developed during carbonization of the CF sample, achieving a V_s of 0.20 cm^3/g and apparent surface area (A_{BET}) of more than 500 m^2/g. These values are lower than those reported for carbonized pure Alcell ® lignin fibers [52]. The similar micropore volume derived from the N_2 and CO_2 adsorption isotherms suggests the presence of narrow porosity, with micropore sizes around 0.7 nm [54]. For most of the metal-containing carbon fibers, the adsorption of N_2 was almost negligible. However, these samples retain the same micropore volume determined by CO_2 adsorption as that of the CF. These differences can be associated with diffusional problems inside narrow micropores (<0.7 nm), which are not easily accessible for N_2 at such a low adsorption temperature (−196 °C), but available for CO_2 at 0 °C. Particularly, CFNi3, CFNi10, CFPd and CFNiCo presented larger metal nanoparticle sizes, which could be blocking the access to pores larger than 0.7 nm. In the case of CFCo and CFNiPd, which have the finest distribution of the metallic phases, these pores may be partially accessible, showing almost half of the micropore volume determined by N_2 adsorption than that of the metal-free carbon fibers.

Table 3 also contains the surface and bulk concentrations measured by XPS and XRF, respectively. Bulk concentrations are close to the nominal metal concentration values for each electrocatalyst. However, the discrepancy between XRF and XPS results suggests that the distribution of nickel on the surface of CFNi3 and CFNi10 is not homogeneous, being this concentrated on the inner surface of the carbon fibers. To verify that the nickel has been homogeneously distributed throughout the carbon fiber radius, an XPS depth profile analysis with Ar sputtering was performed (Fig. S5B). Nickel mass concentration increases with the sputtering time, suggesting that the concentration of nickel inside the fiber is higher than that on the fiber external surface. The same conclusion can be made for CFCo sample. Differently, the Pd-containing carbon fiber catalysts, which showed some roughness in SEM images that were identified as surface metal nanoparticles in TEM, have a larger Pd XPS surface concentration, Table 3, reaching values three

Table 3
Porosity parameters, surface (XPS) and bulk (XRF) mass concentration of the carbon fibers.

Sample		CF	CFNi3	CFNi10	CFCo	CFPd	CFNiCo	CFNiPd
N_2 ads-desorp isotherm								
A_{BET}	(m^2/g)	505	5	5	350	5	5	350
V_{meso}	(cm^3/g)	0.01	<0.01	<0.01	0.03	0.01	0.01	0.03
V_s	(cm^3/g)	0.20	<0.01	<0.01	0.13	0.01	<0.01	0.13
CO_2 ads isotherms								
V_{DR}	(cm^3/g)	0.22	0.21	0.21	0.21	0.21	0.20	0.22
XPS (% wt)								
	C	90.9	93.1	91.6	83.2	87.8	87.4	86.9
	O	6.0.	4.3	5.7	13.3	7.0	9.5	6.6
	N	3.1.	1.9	1.5	2.2	1.8	1.7	1.8
	Ni	<0.1.	0.7	1.2	<0.1	<0.1	0.2	1.6
	Co	<0.1.	<0.1	<0.1	1.3	<0.1	1.2	<0.1
	Pd	<0.1.	<0.1	<0.1	<0.1	3.4	<0.1	3.1
XRF (% wt)								
	Ni	–	3.8	9.3	–	–	1.1	1.1
	Co	–	–	–	3.9	–	4.3	–
	Pd	–	–	–	–	2.9	–	2.9

times higher than those of Ni and Co. In the case of the bi-metallic catalyst, two different behaviors are observed, i) Ni and Co in CFNiCo are mainly concentrated inside the fiber, ii) CFNiPd presents similar Ni & Pd mass concentrations determined by XPS and XRF, evidencing a homogeneous distribution for the metallic particles in them.

On the other hand, all the samples present N surface functional groups, mainly in the form of pyrrole and pyridone (ac. 400.7 eV) and pyridine (398.5 eV) [62], derived from the use of PVP as additive (Fig. S5C). Fig. S6 shows the oxidation states of the metals present in the carbon fiber-based electrocatalysts. It is worth noting that both Ni and Pd present in the carbon fibers are totally reduced to Ni^0 and Pd^0 respectively due to the carboreduction produced during carbonization at 900 °C [63,64]. However, Co shows a more oxidized state probably due to its homogeneous distribution in the fiber, which facilitates its rapid oxidation to CoO and Co_3O_4 after exposure to an oxidizing atmosphere [40].

The striking advantages of using electrospun fiber mats as electrodes become evident during the electrochemical characterization. For this purpose, the samples do not need to be processed through multiple steps, such as preparing an ink or slurry, adding conductivity-enhancing additives or binders, and conducting deposition and controlled drying processes. Simply, the sample mats are cut to an appropriate size to fit into the electrical contact, as described in the experimental section. In this way, cyclic voltammetry (CV) experiments were carried out to evaluate the performance of the electrocatalysts for electrochemical lignin oxidation at room temperature.

Fig. 3 shows the third cycle of the voltammograms recorded on CFNi10, CFPd, CFNiPd and CFCo electrodes. In the absence of lignin, the CFNi10 electrode shows a square-box CV at potentials between −0.6 and −0.1 V related to the formation of the electrical double layer capacitance on the narrow microporosity of the electrode, which is known to enhance the capacitive response of carbon materials [65]. When potential increases, the surface of the carbon fibers is positively polarized, and the capacitive response is suppressed due to the so-called ion sieving effect on the solvated anions, which cannot fit into the narrow micropores of these samples [66]. Nickel electrodes are known to form a Ni $(OH)_2$ layer at the electrode surface under alkaline conditions that acts as electrocatalyst for lignin oxidation [67]. The CV points out that reversible nickel oxidation is feasible on CFNi10, as indicated by the presence of redox peaks at −0.1/0 V (oxidation of Ni to NiOH) and 0.2/0.3 V (Nickel hydroxide is oxidized to NiO), as well as a shoulder at 0.7 V related to the oxyhydroxide nickel formation. When potential gets closer to 0.8 V, a strong oxidation current corresponding to the oxygen evolution reaction is found. In this process an intermediate nickel peroxide ($NiOO_2$) is formed from NiOOH, releasing oxygen radicals such as hydroperoxides [68] and molecular oxygen [69].

As shown in Fig. 3, an irreversible anodic current is found at potentials higher than 0.3 V, when lignin is added to the solution, which has been either associated to the direct electrooxidation of lignin [70] or to the electrooxidation of the products derived from its depolymerization [71]. All the electrochemical processes observed in the experiment with CFNi10 as working electrode, are also found in the CFNi3 sample, but to a lesser extent (CV not shown). Similarly, the CV of the CFPd electrocatalyst shows the redox processes associated with the electroactivity of Pd, and it also delivers an irreversible oxidation current at potentials higher than 0.4 V in the presence of lignin, Fig. 3B. However, the intensity of the electrooxidation process is attenuated with respect to that of CFNi10. The bimetallic CFNiPd electrode presents a similar electrochemical response, Fig. 3C, although the intensity of the electrooxidation process increases, while the onset potential of the process is improved. Finally, the voltammograms of CFCo shows no changes in the electrochemical response when lignin is added to the solution, suggesting that this material is not active for the electrooxidation of lignin at these operating conditions. Consequently, the CFNi10 and CFNiPd samples have been selected to be tested as electrocatalysts for the lignin electrooxidation studies in the electrolyzer reactor.

3.3. Electrooxidation experiments

3.3.1. Direct electrooxidative depolymerization of lignin

Direct electro-oxidative depolymerization should be performed at potentials higher than those observed in the cyclic voltammetry when

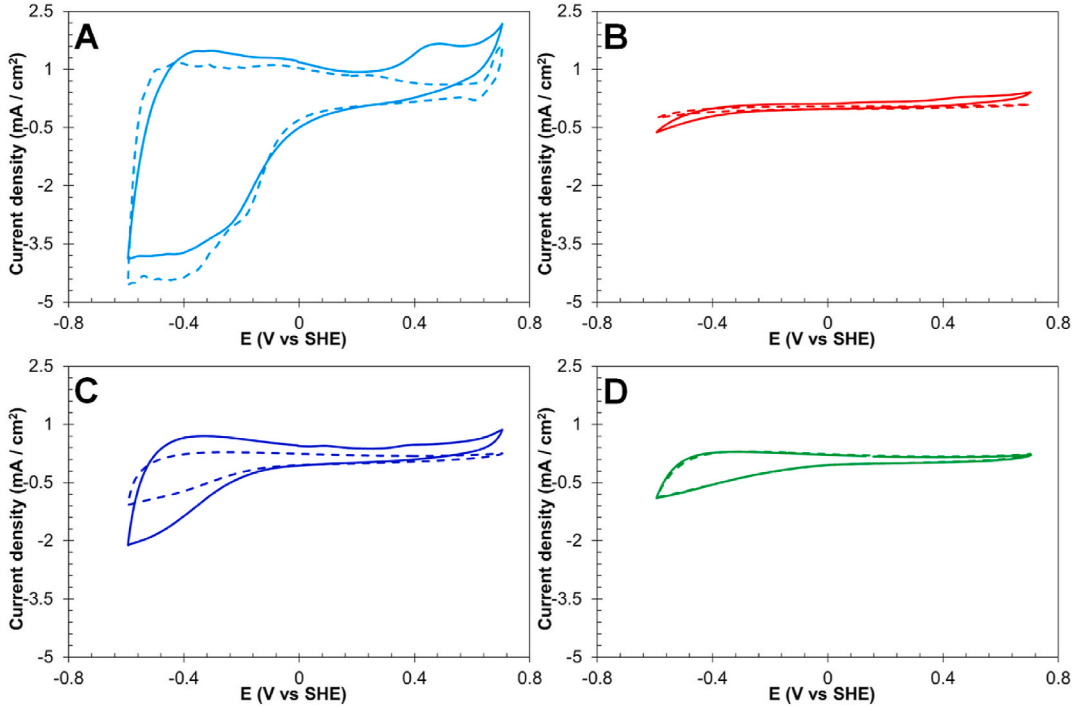

Fig. 3. Cyclic voltammetry of A) CFNi10, B) CFPd, C) CFNiPd and D) CFCo electrodes in 1 M NaOH, at 10 mV/s of scan rate and room temperature. Dashed line: no lignin in the solution; solid line: IND Lignin concentration of 5 g/L.

lignin is added to the alkaline solution (see oxidation peaks in Fig. 3) [72,73]. Previous studies have shown that electrochemical depolymerization of lignin using nickel-based catalysts is very promising, in view of the ability of these materials to selectively cleave specific bonds, such as the β-O-4 ones, and to improve lignin oxidation kinetics, while facilitating more energy-efficient integration with hydrogen production compared to conventional water electrolysis [74–76]. A first attempt was made to study direct electro-oxidative depolymerization of IND lignin in 1 M NaOH. To this end, the experimental setup was set as depicted in Fig. S1B, using the CFNi10 and CFNiPd mats as positive electrode and bare CF mat as negative electrode. The potential of the latter electrode was set to 0.6 V vs SHE in accordance with the CV recorded in the electrochemical characterization of the electrocatalysts.

Liquid samples were taken from the solution tank at different times and analyzed by GC-MS. The corresponding GC-MS chromatogram of the sample obtained after 30 min is shown in Fig. S7. The main monomeric products obtained were vanillin (39.154 min) and guaiacol (13.521 min). Acetovanillone (21.478 min), isovanillic acid (32.666 min), homovallinic acid (37.325 min), 4-Acetyl-2-methoxyphenyl acetate (41.772 min), 4-(4-hydroxy-3 methoxyphenyl)-2-butanone (45.220 min) and ethyl vanillyl ether (48.651 min) could be also identified with phenyl ether (59.984 min) as the only identified dimer, although in a less extent.

Fig. 4 summarizes the vanillin, guaiacol and total monomer concentrations observed for the CFNiPd and CFNi10 electrocatalysts under different reaction times at 0.6 V vs SHE. For the sake of comparison, it also includes the concentration of the compounds obtained without applying any current after 1 h at room temperature. These compounds are produced by the cleavage of the three-dimensional and cross-linked structure of lignin caused by the alkalinity of the reaction medium, a process known as alkaline homolysis. Vanillin yield increases from 0.4 % wt in the homolytic process up to 0.7 % wt for CFNi10 after 5 min. Longer oxidation times up to 120 min did not render any net gain on yield. The promoted vanillin formation along with the suppressed production of guaiacol notably enhances vanillin selectivity from a $S_{Vanillin}$ = 55 % wt for the homolytic reaction to $S_{Vanillin}$ = 83 % wt with CFNi10. CFNiPd sample shows similar catalytic activity to that of CFNi10, being slightly more selective to vanillin ($S_{Vanillin}$ = 86 % wt). Finally, the solid recovered at the end of the reaction accounted for 96–97 % wt of the initial lignin weight, being insoluble in deionized water.

These results suggest that, under the studied conditions, lignin is not depolymerized by promoted cleavage of lignin linkages by electrooxidation. Alternatively, lignin alkaline homolysis seems to drive the depolymerization rate. Any yield increase is probably related to the oxidation of β-O-4 bonds of oligomeric G-containing fragments into guaiacol and vanillin that are likely formed by homolytic breakup of the lignin structure. These oligomers, likely dimers and trimers, can effectively diffuse to the electrode surface and adsorb into the active sites, enabling the catalytic breakage of the bond. Indeed, some of the results that reports direct lignin electrooxidation are focused on model dimer molecules [72]. The linkages allocated within the complex three-dimensional structure of the lignin polymer is not accessible to be cleaved by the metal nanoparticles on the surface of the electrocatalysts due to the obvious steric hindrance. Under such considerations, if lignin depolymerization is to be promoted, the only viable pathways would be those based in mediated mechanisms [26,56], where oxidants are either formed or regenerated in the solution, cleaving lignin bonds at faster rate.

3.3.2. *Electrical-chemical ROS-assisted depolymerization of IND lignin*

Given that homolysis of lignin at room temperature is not sufficient to promote lignin depolymerization, a second lignin depolymerization attempt was made in the same experimental setup by using higher currents during the galvanostatic treatment. For this study, CFNi10 was chosen, since it showed the most promising results on the previous electrooxidation test. Fig. 5 compiles the time evolution of the yield to vanillin and other monomers achieved at 100, 200 and 400 mA.

The evolution of the monomeric yield with time at 100 mA, Fig. 5A, reveals that the ROS-assisted depolymerization can increase the vanillin up to 1 % wt and total monomer production to 1.4 % wt. These results confirm that depolymerization must be promoted to release additional oligomers and monomers that can be converted into aromatic monomers by the active sites of CFNi10 catalyst. Both the yields of vanillin and total monomers increased initially, reaching a maximum of 0.95 and 1.40 % wt after 105 min, respectively, Fig. 5A. Thereafter, a steady decrease in the concentration of monomers, other than vanillin, was observed [70]. Consequently, vanillin selectivity (g of vanillin per g of quantified monomers in solution) ranges from 55 to 72 % wt, increasing with time due to the higher degradation rate of the other monomers, especially guaiacol.

The degradation of the lignin monomers is related to the overoxidation towards organic acids and/or even their total mineralization (i.e CO_2 formation). Decomposition takes places preferentially with guaiacol and other marginal guaiacol-derived monomers, since they have been reported to be more easily degraded under anodic oxidation than vanillin [56]. These results show that the compounds of interest should be extracted from the solution to avoid their degradation, a viable approach that has been explored, elsewhere, by coupling ultrafiltration membranes to flow-through electrochemical cells [12]. Note that vanillin selectivity has decreased from the 85 % wt value obtained under the use of softer operation conditions, Fig. 4, stressing the relevance of selecting operating conditions that matches the downstream separation process. The absence of leaching of nickel from the CFNi10 fiber was analyzed by measuring the Ni content in the reaction medium after 6 h of electrooxidation by inductively coupled plasma mass spectrometry (ICP-MS), where the presence of Ni was not detected (detection limit of 1.3 mg/kg), and by XRF analysis of the electrocatalyst after the reaction, obtaining a value of nickel content similar to the initial one, i.e. 9.2 % wt of Ni after reaction vs. 9.3 % wt of Ni in the fresh electrocatalyst (Table 2).

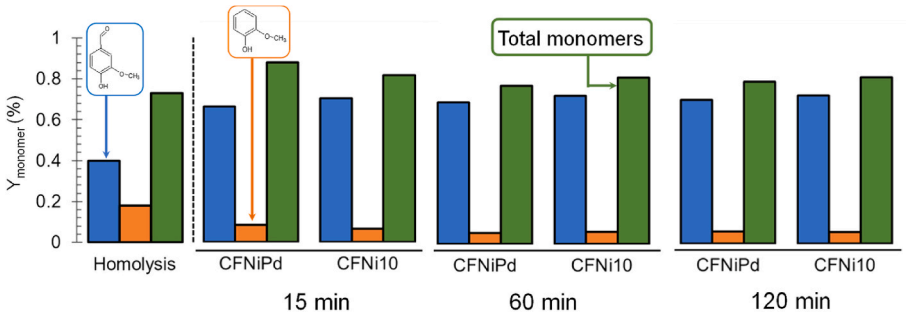

Fig. 4. Yields to vanillin (blue), guaiacol (orange) and total monomers (green) during the depolymerization of lignin in 1 M NaOH without working electrode (Homolysis), and with CFNiPd and CFNi10 as working electrode at different electrochemical reaction times. Electrode potential: 0.6 V vs SHE. IND Lignin concentration: 25 g/L. (For interpretation of the references to colour in this figure legend, the reader is referred to the Web version of this article.)

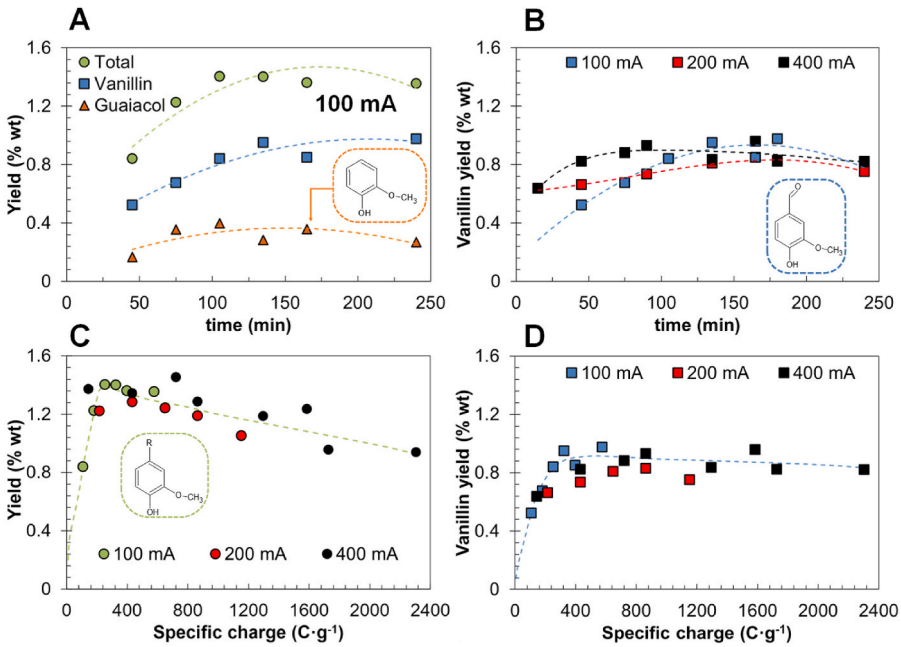

Fig. 5. A) Vanillin, guaiacol and total monomer produced during electrooxidation treatment of lignin using CFNi10 | CF electrodes as a function of time. B) Effect of current intensity on vanillin yield. C, D) Evolution of the total monomeric and vanillin yields, respectively, with the specific charge dosed during electrooxidation of lignin. Current intensity: 100 mA, IND lignin concentration: 25 g/L.

When the intensity of the applied current is increased, the vanillin production is speeded up, achieving the maximum vanillin production at shorter times, 70 min at 400 mA vs 120 min at 100 mA (Fig. 5B). Although the rate of vanillin production increases with the applied current, the maximum value reached at 100 mA cannot be exceeded, evidencing that, by simply raising the applied current, vanillin production cannot be promoted. On the other hand, Fig. 5B also shows the stability of the process in terms of vanillin production, which does not decrease even at the highest applied current after 200 min.

The yields obtained at different currents and expressed in terms of specific charge are plot together in Fig. 5C and D. Vanillin yield stops to increase beyond 300C/g, no matter the intensity current used, while total monomeric yield decreases at dosing charges higher than 400C/g. These results suggest an optimum of specific charge between 300 and 400C/g, when the electrochemical process is focused on the production of monomers of interest, rather than on lignin depolymerization. Specifically, Fig. 5D shows that the reaction carried out at 100 mA reaches the maximum vanillin yield at lower dosing charges compared to those at 200 and 400 mA, meaning that a lower energy input requirement is needed at 100 mA to reach the optimal reaction yield. This could be attributed to the likely increase in the formation of reactive oxygen species through competitive reactions at higher current intensities, which would consume part of the applied energy. In addition, the increased presence of ROS could not only promote further depolymerization of lignin, but also contribute to a slight degradation of vanillin [77]. The generation of additional monomers by the latter reactions would partially compensate for the higher monomeric degradation rate, which would explain the slightly higher total monomeric yield, when compared to the evolution of yields at 200 mA.

3.3.3. *Electrochemical H_2O_2-assisted depolymerization of IND lignin*

It is worth noting that hydrogen peroxide-mediated oxidation has been previously explored using Ni-based materials, achieving satisfactory results in lignin depolymerization without the use of anodic oxidation. Thus, recent studies have shown that the combination of Ni with other catalysts under mild oxidation conditions with H_2O_2 can significantly enhance the scission of lignin bonds, resulting in the production of specific monomeric phenols [78,79]. Following this line, the electrochemical depolymerization of lignin can be also promoted via the formation of hydrogen peroxide from oxygen reduction at the cathode, an approach that has been already reported in the literature with successfully results [26]. A commercial Nickel foam and Toray carbon fiber paper were used as positive and negative electrodes, respectively, for the sake of comparison.

Bearing this idea in mind, the tank containing the lignin solution was bubbled with O_2 in order to saturate the solution with oxygen and the lignin solution was forced to physically pass through the vicinity of the negative electrode, where metal-free lignin-based carbon fibers were used as electrode, as depicted in Fig. S1D. It is known that bare carbon surface as well as carbon felts consisting of carbon microfibers (similar to those present in the CF carbon mats but having larger diameters) are consistently used to implement electrochemical generation of H_2O_2 for oxidation processes because they catalyze the 2 e^- ORR pathway through the following reaction: $O_2 + 2H_2O + 2\ e^- \rightarrow H_2O_2 + 2OH$ [80, 81]. CFNi10 was again used as positive electrode. Given the stronger oxidative conditions expected on this cell configuration and the lower power consumption, the current intensity was set to 100 mA.

The evolution of the monomer yields with time and specific charge are reported in Fig. 6. The injection of oxygen during the treatment has a strong impact on the kinetic rate of the process, enhancing the formation of monomers at short times, with vanillin and total yields increasing by 63 %, after 45 min of reaction. Vanillin yield reaches a maximum value of 1.10 % wt after 135 min, showing a turnover rate of 38.75 $mol_{Vanillin}/mol_{Ni\ surface}/h$. A higher improvement is observed for total monomeric yield, 1.41 % wt, due to the severe depolymerization conditions. A slightly larger and broader product distribution at short reaction times (vanillin selectivity of 55 % wt) is obtained, due to the unselective oxidation reactions promoted by H_2O_2 [26]. However, the degradation rate of monomers different from lignin is much faster, as exemplified by the significant decline in guaiacol yield with reaction time observed in Fig. 6A. The oxidation of these monomers leads to an increase in vanillin selectivity, reaching a value of 78 % after 2 h.

In addition, the optimum specific charge value is obtained at 325 C/g, in agreement with the 300–400 C/g window observed in the ROS-assisted treatment (absence of O_2). Although the yield towards vanillin is comparable to those previously reported under similar

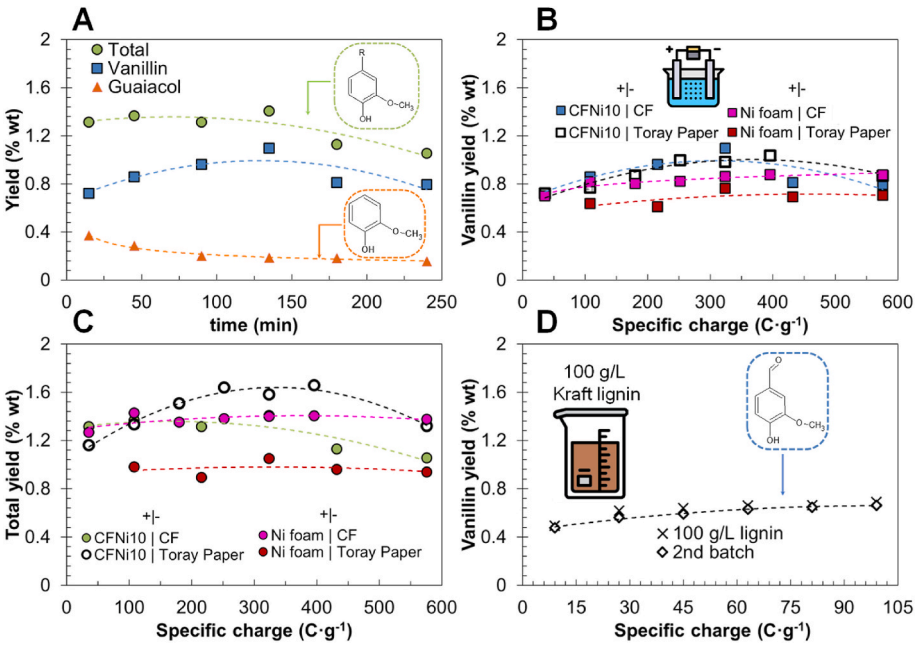

Fig. 6. A) monomer yields as a function of time for the electrochemical oxidation of lignin in the presence of O_2. Current intensity: 100 mA, lignin concentration: 25 g/L. B,C) vanillin and total yields, respectively as a function of specific charge for the electrochemical oxidation of lignin in the presence of O_2 using CFNi10 | CF, CFNi10 | Toray Paper, Ni foam | CF and Ni foam | Toray Paper as positive and negative electrodes: 100 mA, IDN lignin concentration: 25 g/L. D) Vanillin yield as a function of specific charge for the electrochemical oxidation of lignin in the presence of O_2, with a lignin concentration of 100 g/L and the reutilization of the CFNi10 | CF electrodes for a second lignin batch. Current intensity: 100 mA, O_2-saturated electrolyte.

conditions using IND lignin and Ni, Co, Fe, or Ti electrodes, the electrocatalysts presented in this study are more sustainable, have lower metal loading and are obtained by a simpler and cost-reduced synthesis process [12,71,82].

Furthermore, CFNi10 electrocatalyst presents a similar activity to that observed for an activated Ni foam anode, but requires much lower energy consumption (around 5 times lower C/g_{lignin}) [82], while using a two orders of magnitude lower amount of nickel (ca. of 1 mg of Ni in CFNi10 self-standing electrode vs 110–130 mg of Ni in Ni foam catalyst). Moreover, although some studies have used expensive deposition methods to synthesize Ni-based electrocatalysts on carbon supports, these approaches result in significantly lower vanillin production, with mass yields of less than 1 % [83]. The total yield of aromatics is also in line with those reported in the literature, where typically mass yields for this technical lignin are under 2 % wt [84].

The solid yield and total amount of water-soluble depolymerized products obtained after 4h at 400 mA under N_2 and after 4h at 100 mA under O_2 has been determined as described in section 2.4.2. Solid yields of 72.5 % wt and water-soluble depolymerized products yield of 19.8 % wt have been determined via ROS-assisted depolymerization, while 77.2 % wt and 13.7 % wt, respectively, were obtained under the H_2O_2-assisted approach. Initially, these results suggest that H_2O_2-assisted approach is more effective for promoting lignin depolymerization, since this technique uses 4-times less charge. However, additional experiments would be needed to optimize the operating conditions that restrict potentially excessive mineralization of the lignin feedstock.

The performance of the electrospun electrocatalysts has been compared against that of commercial electrodes, i.e. Nickel foam as positive electrode and Toray Carbon Paper as negative electrodes, showing a superior performance in terms of vanillin yield (blue vs purple dots in Fig. 6B). The nickel surface area reported by the Nickel foam supplier is 2.2 m^2/g, while the estimated surface area of nickel nanoparticles on CFNi10, supposing spherical particles and attending to the Ni loading obtained by XRF and the average Ni nanoparticle from TEM images, is 3.2 m^2/g, suggesting that the surface area is comparable between these samples (although using 100 times lower amount of nickel in CFNi10 electrode). Note that the nickel specific loading in the cell has been decreased from 30 mg/cm^2 (Ni Foam) down to 0.3 mg/cm^2 (CFNi10), notably decreasing the need of using a critical mineral as active phase.

The improved vanillin yield might be related to a better distribution of nickel in CFNi10, which renders a localized ROS production for lignin depolymerization, while enabling selective oxidation of dimer and oligomer β-O-4 bonds, demoting the overoxidation processes. CFNi10 electrode seems to be the responsible for the improved vanillin selectivity attained during the process, as pointed out by the similar catalytic performance when the CF cathode was replaced by Toray Carbon Paper, (Fig. 6B, black dots). In fact, when the total monomer yields are compared, Fig. 6C, the pair CFNi10 | Toray Carbon Paper achieves higher values than CFNi10 | CF, showing an increase of almost 0.2 % wt, indicating that CF likely fosters the overoxidation of monomers due to a higher H_2O_2 production.

As a final test, the lignin concentration on the tank was increased to 100 g/L. The higher lignin concentration seems to hinder vanillin production, Fig. 6D, showing a vanillin yield of 0.69 % wt at 100C/g vs 0.85 % wt for the same specific charge, but using 25 g/L. The reusability of the electrodes was tested on this experiment by cleansing the cell with 100 mL of 1 M NaOH and refreshing the 100 g/L lignin solution After cleaning of the electrochemical cell and replacing the lignin solution in the tank, the electrospun electrocatalysts were able to successfully produce vanillin and monomers at similar rates in the second cycle, Fig. 6D, evidencing the stability and reusability of the electrodes at the operating conditions studied.

3.4. *Residual lignin characterization*

After the electrooxidation reaction using Ni loaded carbon fiber based electrocatalyst at 200 mA for 2 h, the electrooxidated lignin (EOL) was isolated and recovered as previously described in section 2.4.2.

Fig. 7A shows the GPC data of EOL. The final lignin product shows an average molecular weight of 840 Da, being eight times lower than that of the starting sample, Table 1, proving that the electrochemical treatment

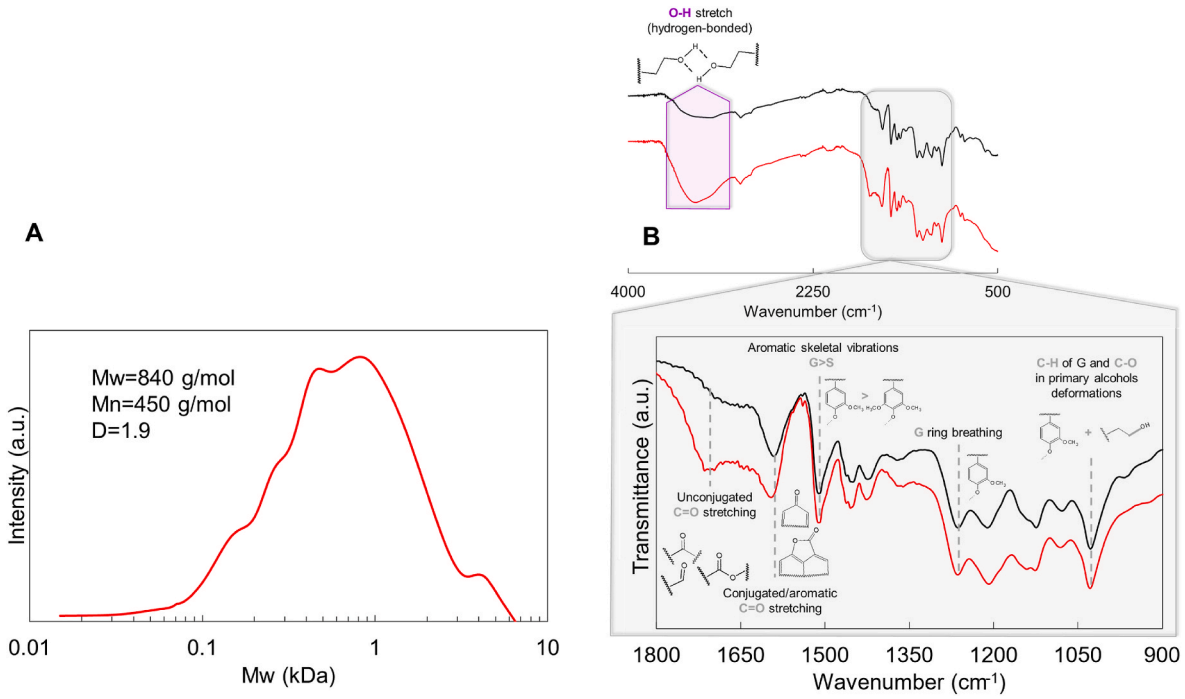

Fig. 7. A) GPC analysis of electrooxidated lignin and B) FT-IR spectra of Kraft lignin (black line) and electrooxidated lignin (red line). (For interpretation of the references to colour in this figure legend, the reader is referred to the Web version of this article.)

leads to a strong decrease of average molecular weight. In addition, the polydispersity of the lignin is also altered by the electrochemical treatment, decreasing from roughly 9.9 to 1.9, pointing out that the product solid phase is mainly composed of small size oligomeric compounds. The ultimate analysis results reveals that a large amount of oxygenated groups are inserted into the molecular structure of the solid product, showing an increase on the oxygen content from 29.7 % wt in the fresh IND lignin (Table 1) to 36.1 % wt for the EOL.

The EOL was further analyzed to understand the nature of the new oxygenated groups. Fig. 7B shows the FTIR spectrum of lignin before and after electrooxidation. A strong increase in the intensity of the region between 3700 and 3200 cm^{-1} for EOL is observed [85], associated with the stretching of the O-H bond (hydrogen bonded), suggesting that hydroxyl groups have been introduced during the electrooxidation treatment. Likewise, EOL shows a more accentuated peak at 1700 cm^{-1} due to the presence of C=O bonds in the non-conjugated species, while no clear difference between the lignin before and after reaction can be appreciated in the region related to the stretching in the carbonyl groups in aromatic or conjugated species, 1590 cm^{-1} [86]. This effect can be associated with the oxidation of side chains under the mild reaction conditions, which prevails over the oxidation of aromatic units.

The decrease in the average molecular weight and the generation of hydroxyl and carbonyl functional groups on the residual lignin might allow its use in different applications such as the production of polyurethanes, where raw technical lignins are usually subjected to oxypropylation, etherification and depolymerization treatments to obtain a material with low molecular weight and high content of oxygenated hydroxyl and carbonyl groups [2]. In this sense, Conde et al. recently demonstrated that Organosolv lignin can be electrochemically oxidized to produce a decrease on their molecular weight, allowing the use of the modified lignin as bioadhesive precursor, although boron-doped diamond electrodes were utilized as electrocatalysts [87]. This result validates the complete valorization of the feedstock and open the door to fine tune the electrochemical oxidation conditions in order to modify the lignin by grafting new functional groups, rather than favoring the depolymerization process.

4. Conclusion

Non-woven mats consisting of metal-containing lignin nanofibers were obtained by electrospinning of lignin/PVP and Ni, Co or Pd solutions in only one step. These mats were tested as self-standing electrodes, without additives and further processing, for the first time in the electrochemical depolymerization of kraft lignin. The catalyst prepared with 10 % wt Ni showed the highest activity, in a filter-press electrolyzer cell, operating at room temperature and using specific currents of 25–100 mA/cm^2, for 0–4 h, with 25–100 g_{Lignin}/L of O_2-saturated alkaline solutions. The electrospun CF10Ni catalyst showed higher yields towards aromatic production than commercial nickel foams, while using 100 times lower amount of the active phase. The characterization of the residual depolymerized lignin solid suggested a high potential as raw material for different value-added polymeric material applications.

CRediT authorship contribution statement

M. García-Rollán: Writing – original draft, Resources, Methodology, Investigation, Formal analysis. **M. Toscano-de los Riscos:** Visualization, Methodology, Investigation. **R. Ruiz-Rosas:** Writing – review & editing, Visualization, Supervision, Methodology, Formal analysis, Conceptualization. **J.M. Rosas:** Writing – review & editing, Supervision, Project administration, Funding acquisition. **J. Rodríguez-Mirasol:** Supervision, Project administration, Funding acquisition. **T. Cordero:** Supervision, Methodology, Funding acquisition, Conceptualization.

Acknowledgements

The authors wish to thank MICINN (TED-2021-131324B-C21 at MCIN/AEI/10.13039/501100011033, "Next GenerationEU"/PRTR) and Junta de Andalucía (UMA18-FEDERJA-110) for financial support. M.G.R. acknowledges the assistance of MICINN through an FPU Grant (FPU18/01402).

Appendix A. Supplementary data

Supplementary data to this article can be found online at https://doi.org/10.1016/j.biombioe.2024.107560.

Data availability

No data was used for the research described in the article.

References

[1] J. Zakzeski, P.C.A. Bruijnincx, A.L. Jongerius, B.M. Weckhuysen, The catalytic valorization of lignin for the production of renewable chemicals, Chem. Rev. 110 (2010) 3552–3599, https://doi.org/10.1021/cr900354u.

[2] S. Mastrolitti, E. Borsella, A. Giuliano, M. Petrone, I. De Bari, R. Gosselink, G. van Erven, E. Annevelink, K. Triantafyllidis, H. Stichnothe, H. Lange, G. Bell, Sustainable Lignin Valorization Technical Lignin, Processes and Market Development, 2021.

[3] H. Guo, Y. Zhao, J.S. Chang, D.J. Lee, Lignin to value-added products: research updates and prospects, Bioresour. Technol. 384 (2023) 129294, https://doi.org/10.1016/J.BIORTECH.2023.129294.

[4] Q. Tian, P. Xu, D. Huang, H. Wang, Z. Wang, H. Qin, Y. He, R. Li, L. Yin, S. Chen, Y. Zhao, The driving force of biomass value-addition: selective catalytic depolymerization of lignin to high-value chemicals, J. Environ. Chem. Eng. 11 (2023) 109719, https://doi.org/10.1016/J.JECE.2023.109719.

[5] J.M. Rosas, R. Berenguer, M.J. Valero-Romero, J. Rodríguez-Mirasol, T. Cordero, Preparation of different carbon materials by thermochemical conversion of lignin, Front Mater 1 (2014) 29, https://doi.org/10.3389/FMATS.2014.00029/BIBTEX.

[6] M. García-Rollán, F.J. García-Mateos, R. Ruiz-Rosas, J.M. Rosas, J. Rodríguez-Mirasol, T. Cordero, MgO-containing porous carbon spheres derived from magnesium lignosulfonate as sustainable basic catalysts, J. Environ. Chem. Eng. 11 (2023) 109060, https://doi.org/10.1016/J.JECE.2022.109060.

[7] R.J. Khan, C.Y. Lau, J. Guan, C.H. Lam, J. Zhao, Y. Ji, H. Wang, J. Xu, D.J. Lee, S. Y. Leu, Recent advances of lignin valorization techniques toward sustainable aromatics and potential benchmarks to fossil refinery products, Bioresour. Technol. 346 (2022) 126419, https://doi.org/10.1016/J.BIORTECH.2021.126419.

[8] M. Chen, J. Zhang, Y. Wang, Z. Tang, J. Shi, C. Wang, Z. Yang, J. Wang, H. Zhang, Lignin catalytic depolymerization for liquid fuel and phenols by using Mo/sepiolite catalysts calcined at different temperature, J. Environ. Chem. Eng. 9 (2021) 105348, https://doi.org/10.1016/J.JECE.2021.105348.

[9] O. Movil-Cabrera, A. Rodriguez-Silva, C. Arroyo-Torres, J.A. Staser, Electrochemical conversion of lignin to useful chemicals, Biomass Bioenergy 88 (2016) 89–96, https://doi.org/10.1016/j.biombioe.2016.03.014.

[10] X. Du, H. Zhang, K.P. Sullivan, P. Gogoi, Y. Deng, Electrochemical lignin conversion, ChemSusChem 13 (2020) 4318–4343, https://doi.org/10.1002/CSSC.202001187.

[11] M. Garedew, F. Lin, B. Song, T.M. DeWinter, J.E. Jackson, C.M. Saffron, C.H. Lam, P.T. Anastas, Greener routes to biomass waste valorization: lignin transformation through electrocatalysis for renewable chemicals and fuels production, ChemSusChem 13 (2020) 4214–4237, https://doi.org/10.1002/CSSC.202000987.

[12] S. Stiefel, J. Lölsberg, L. Kipshagen, R. Möller-Gulland, M. Wessling, Controlled depolymerization of lignin in an electrochemical membrane reactor, Electrochem. Commun. 61 (2015) 49–52, https://doi.org/10.1016/J.ELECOM.2015.09.028.

[13] P. Cai, H. Fan, S. Cao, J. Qi, S. Zhang, G. Li, Electrochemical conversion of corn stover lignin to biomass-based chemicals between Cu/NiMoCo cathode and Pb/PbO_2 anode in alkali solution, Electrochim. Acta 264 (2018) 128–139, https://doi.org/10.1016/J.ELECTACTA.2018.01.111.

[14] D. Di Marino, T. Jestel, C. Marks, J. Viell, M. Blindert, S.M.A. Kriescher, A. C. Spiess, M. Wessling, Carboxylic acids production via electrochemical depolymerization of lignin, Chemelectrochem 6 (2019) 1434–1442, https://doi.org/10.1002/CELC.201801676.

[15] S. Stiefel, A. Schmitz, J. Peters, D. Di Marino, M. Wessling, An integrated electrochemical process to convert lignin to value-added products under mild conditions, Green Chem. 18 (2016) 4999, https://doi.org/10.1039/c6gc00878j.

[16] R.C.P. Oliveira, J.G. Buijnsters, M.M. Mateus, J.C.M. Bordado, D.M.F. Santos, On the electrooxidation of kraft black liquor on boron-doped diamond, J. Electroanal. Chem. 909 (2022) 116151, https://doi.org/10.1016/J.JELECHEM.2022.116151.

[17] A.M.B. Honorato, M. Khalid, A.A. da S. Curvelo, H. Varela, S. Shahgaldi, Trimetallic nanoalloy of NiFeCo embedded in phosphidated nitrogen doped carbon catalyst for efficient electro-oxidation of kraft lignin, Polymers 14 (2022) 3781, https://doi.org/10.3390/POLYM14183781/S1.

[18] X. Du, H. Zhang, K.P. Sullivan, P. Gogoi, Y. Deng, Electrochemical lignin conversion, ChemSusChem 13 (2020) 4318–4343, https://doi.org/10.1002/CSSC.202001187.

[19] Z. Fang, J.E. Jackson, E.L. Hegg, Mild, electroreductive lignin cleavage: optimizing the depolymerization of authentic lignins, ACS Sustain. Chem. Eng. 10 (2022) 7545–7552, https://doi.org/10.1021/acssuschemeng.2c00820.

[20] M.G.A. da Cruz, R. Gueret, J. Chen, J. Piątek, B. Beele, M.H. Sipponen, M. Frauscher, S. Budnyk, B.V.M. Rodrigues, A. Slabon, Electrochemical depolymerization of lignin in a biomass-based solvent, ChemSusChem 15 (2022) e202200718, https://doi.org/10.1002/CSSC.202200718.

[21] Z. Li, M. Garedew, C.H. Lam, J.E. Jackson, D.J. Miller, C.M. Saffron, Mild electrocatalytic hydrogenation and hydrodeoxygenation of bio-oil derived phenolic compounds using ruthenium supported on activated carbon cloth, Green Chem. 14 (2012) 2540–2549, https://doi.org/10.1039/C2GC35552C.

[22] D. di Marino, V. Aniko, A. Stocco, S. Kriescher, M. Wessling, Emulsion electro-oxidation of kraft lignin, Green Chem. 19 (2017) 4778–4784, https://doi.org/10.1039/C7GC02115A.

[23] Q. Zhu, B. Gong, S. Huang, Y. Jin, S. Liu, S. Shao, Y. Yang, T. Cataldo, N. M. Bedford, J.C.H. Lam, Rhombohedral ZnIn2S4-catalysed anodic direct electrochemical oxidative cleavage of C–O bond in α-O-4 linkages in ambient conditions, Green Chem. 26 (2024) 4135–4150, https://doi.org/10.1039/D4GC00338A.

[24] R. Ghahremani, J.A. Staser, Electrochemical oxidation of lignin for the production of value-Added chemicals on Ni-Co bimetallic electrocatalysts, Holzforschung 72 (2018) 951–960, https://doi.org/10.1515/hf-2018-0041.

[25] W. Sun, T.L. Greaves, M.Z. Othman, Effect of inorganic additives and optimisation of the electro-assisted organosolv pretreatment of biomass, J. Environ. Chem. Eng. 9 (2021) 106432, https://doi.org/10.1016/J.JECE.2021.106432.

[26] H. Zhu, Y. Chen, T. Qin, L. Wang, Y. Tang, Y. Sun, P. Wan, Lignin depolymerization via an integrated approach of anode oxidation and electro-generated H_2O_2 oxidation, RSC Adv. 4 (2014) 6232–6238, https://doi.org/10.1039/c3ra47516f.

[27] X. Du, W. Liu, Z. Zhang, A. Mulyadi, A. Brittain, J. Gong, Y. Deng, Low-energy catalytic electrolysis for simultaneous hydrogen evolution and lignin depolymerization, ChemSusChem 10 (2017) 847–854, https://doi.org/10.1002/CSSC.201601685.

[28] B. Xie, Y. Tobimatsu, K. Narita, S. Yokohata, H. Kamitakahara, T. Takano, Electro-oxidation of lignin model compounds and synthetic lignin with transition-metal complexes (manganese and iron complexes), ACS Sustain. Chem. Eng. 10 (2022) 16701–16708, https://doi.org/10.1021/acssuschemeng.2c04811.

[29] A. Dominguez-Ramos, R. Aldaco, A. Irabien, Electrochemical oxidation of lignosulfonate: total organic carbon oxidation kinetics, Ind. Eng. Chem. Res. 47 (2008) 9848–9853, https://doi.org/10.1021/IE801109C.

[30] S. Litster, G. McLean, PEM fuel cell electrodes, J. Power Sources 130 (2004) 61–76, https://doi.org/10.1016/j.jpowsour.2003.12.055.

[31] International Energy Agency, Critical Minerals – Topics - IEA, (n.d.). https://www.iea.org/topics/critical-minerals (accessed March 22, 2024).

[32] J. Xue, T. Wu, Y. Dai, Y. Xia, Electrospinning and electrospun nanofibers: methods, materials, and applications, Chem. Rev. 119 (2019) 5298–5415, https://doi.org/10.1021/acs.chemrev.8b00593.

[33] J.G.R. da Costa, J.M. Costa, A.F. de Almeida Neto, Recent advances and future applications in electro-adsorption technology: an updated review, J. Environ. Chem. Eng. 9 (2021) 106355, https://doi.org/10.1016/J.JECE.2021.106355.

[34] Y. Wen, M.D.R. Kok, J.P.V. Tafoya, A.B.J. Sobrido, E. Bell, J.T. Gostick, S. Herou, P. Schlee, M.M. Titirici, D.J.L. Brett, P.R. Shearing, R. Jervis, Electrospinning as a route to advanced carbon fibre materials for selected low-temperature electrochemical devices: a review, J. Energy Chem. 59 (2021) 492–529, https://doi.org/10.1016/J.JECHEM.2020.11.014.

[35] F.J. García-Mateos, J.M. Rosas, R. Ruiz-Rosas, J. Rodríguez-Mirasol, T. Cordero, Highly porous and conductive functional carbon fibers from electrospun phosphorus-containing lignin fibers, Carbon 200 (2022) 134–148, https://doi.org/10.1016/J.CARBON.2022.08.050.

[36] F.J. García-Mateos, R. Ruiz-Rosas, J. María Rosas, E. Morallón, D. Cazorla-Amorós, J. Rodríguez-Mirasol, T. Cordero, Activation of electrospun lignin-based carbon fibers and their performance as self-standing supercapacitor electrodes, Sep. Purif. Technol. 241 (2020) 116724, https://doi.org/10.1016/J.SEPPUR.2020.116724.

[37] M.C. Ribadeneyra, L. Grogan, H. Au, P. Schlee, S. Herou, T. Neville, P.L. Cullen, M. D.R. Kok, O. Hosseinaei, S. Danielsson, P. Tomani, M.M. Titirici, D.J.L. Brett, P. R. Shearing, R. Jervis, A.B. Jorge, Lignin-derived electrospun freestanding carbons as alternative electrodes for redox flow batteries, Carbon 157 (2020) 847–856, https://doi.org/10.1016/J.CARBON.2019.11.015.

[38] N. Mubarak, F. Rehman, M. Ihsan-Ul-Haq, M. Xu, Y. Li, Y. Zhao, Z. Luo, B. Huang, J.-K. Kim, N. Mubarak, M. Ihsan-Ul-Haq, M. Xu, Y. Li, Y. Zhao, B. Huang, J.-K. Kim, F. Rehman, Z. Luo, Highly sodiophilic, defect-rich, lignin-derived skeletal carbon nanofiber host for sodium metal batteries, Adv. Energy Mater. 12 (2022) 2103904, https://doi.org/10.1002/AENM.202103904.

[39] F.J. García-Mateos, R. Ruiz-Rosas, J.M. Rosas, J. Rodríguez-Mirasol, T. Cordero, Phosphorus containing carbon (submicron)fibers as efficient acid catalysts, Catal. Today 383 (2022) 308–319, https://doi.org/10.1016/j.cattod.2020.10.025.

[40] M.J. Valero-Romero, F.J. García-Mateos, F. Kapteijn, J. Rodríguez-Mirasol, T. Cordero, Fischer-Tropsch synthesis over lignin-derived cobalt-containing porous carbon fiber catalysts, Appl. Catal., B 321 (2023) 122078, https://doi.org/10.1016/J.APCATB.2022.122078.

[41] R. Li, Greenchem, X. Zhao, G. Chemistry, D. Gao, D. Ouyang, Electro-oxidative depolymerization of lignin for production of value-added chemicals, Green Chem. 24 (2022) 8585–8605, https://doi.org/10.1039/D2GC02660K.

[42] H. Zhu, L. Wang, Y. Chen, G. Li, H. Li, Y. Tang, P. Wan, Electrochemical depolymerization of lignin into renewable aromatic compounds in a non-diaphragm electrolytic cell, RSC Adv. 4 (2014) 29917–29924, https://doi.org/10.1039/C4RA03793F.

[43] Z. Han, H. Jiang, A. Xue, G. Ni, Y. Sun, Y. Tang, P. Wan, Y. Chen, H2O2 generated through ORR on cathode in a protic ionic liquid and its utilization in lignin valorization, J. Electroanal. Chem. 923 (2022) 116814, https://doi.org/10.1016/J.JELECHEM.2022.116814.

[44] H. Jiang, L. Wang, L. Qiao, A. Xue, Y. Cheng, Y. Chen, Y. Ren, Y. Chen, P. Wan, Improved oxidative cleavage of lignin model compound by ORR in protic ionic liquid, Int. J. Electrochem. Sci. 14 (2019) 2645–2654, https://doi.org/10.20964/2019.03.10.

[45] H. Jiang, A. Li, Y. Sun, L. Wang, Y. Chen, Enhanced ORR performance to electrochemical lignin valorization in a mixture of ionic liquid/organic solvent binary electrolytes, New J. Chem. 47 (2023) 18682–18689, https://doi.org/10.1039/D3NJ03967F.
[46] L. Wang, S. Liu, H. Jiang, Y. Chen, L. Wang, G. Duan, Y. Sun, Y. Chen, P. Wan, Electrochemical generation of ROS in ionic liquid for the degradation of lignin model compound, J. Electrochem. Soc. 165 (2018) H705–H710, https://doi.org/10.1149/2.0801811JES/XML.
[47] S. Sun, X. Qiu, S. Hao, S. Ravichandran, J. Song, W. Zhang, Electrochemical conversion of lignin to short-chain carboxylic acids, Green Chem. 25 (2023) 3127–3136, https://doi.org/10.1039/D3GC00324H.
[48] F.J. García-Mateos, T. Cordero-Lanzac, R. Berenguer, E. Morallón, D. Cazorla-Amorós, J. Rodríguez-Mirasol, T. Cordero, Lignin-derived Pt supported carbon (submicron)fiber electrocatalysts for alcohol electro-oxidation, Appl. Catal., B 211 (2017) 18–30, https://doi.org/10.1016/J.APCATB.2017.04.008.
[49] N.M. Bedford, M.B. Dickerson, L.F. Drummy, H. Koerner, K.M. Singh, M. C. Vasudev, M.F. Durstock, R.R. Naik, A.J. Steckl, Nanofiber-based bulk-heterojunction organic solar cells using coaxial electrospinning, Adv. Energy Mater. 2 (2012) 1136–1144, https://doi.org/10.1002/AENM.201100674.
[50] I.G. Loscertales, A. Barrero, I. Guerrero, R. Cortijo, M. Marquez, A.M. Gañán-Calvo, Micro/nano encapsulation via electrified coaxial liquid jets, Science 295 (2002) 1695–1698, https://doi.org/10.1126/science.1067595.
[51] J.L. Braun, K.M. Holtman, J.F. Kadla, Lignin-based carbon fibers: oxidative thermostabilization of kraft lignin, Carbon 43 (2005) 385–394, https://doi.org/10.1016/J.CARBON.2004.09.027.
[52] R. Ruiz-Rosas, J. Bedia, M. Lallave, I.G. Loscertales, A. Barrero, J. Rodríguez-Mirasol, T. Cordero, The production of submicron diameter carbon fibers by the electrospinning of lignin, Carbon 48 (2010) 696–705, https://doi.org/10.1016/j.carbon.2009.10.014.
[53] R. Berenguer, F.J. García-Mateos, R. Ruiz-Rosas, D. Cazorla-Amorós, E. Morallón, J. Rodríguez-Mirasol, T. Cordero, Biomass-derived binderless fibrous carbon electrodes for ultrafast energy storage, Green Chem. 18 (2016) 1506–1515, https://doi.org/10.1039/C5GC02409A.
[54] M. Thommes, K. Kaneko, A.V. Neimark, J.P. Olivier, F. Rodriguez-Reinoso, J. Rouquerol, K.S.W. Sing, Physisorption of gases, with special reference to the evaluation of surface area and pore size distribution (IUPAC Technical Report), Pure Appl. Chem. 87 (2015) 1051–1069, https://doi.org/10.1515/pac-2014-1117.
[55] J. Jagiello, C. Ania, J.B. Parra, C. Cook, Dual gas analysis of microporous carbons using 2D-NLDFT heterogeneous surface model and combined adsorption data of N_2 and CO_2, Carbon 91 (2015) 330–337, https://doi.org/10.1016/j.carbon.2015.05.004.
[56] P. Parpot, A.P. Bettencourt, A.M. Carvalho, E.M. Belgsir, Biomass conversion: attempted electrooxidation of lignin for vanillin production, J. Appl. Electrochem. 30 (2000) 727–731, https://doi.org/10.1023/A:1004003613883/METRICS.
[57] D. Guo, R. Shibuya, C. Akiba, S. Saji, T. Kondo, J. Nakamura, Active sites of nitrogen-doped carbon materials for oxygen reduction reaction clarified using model catalysts, Science 351 (2016) 361–365, https://doi.org/10.1126/science.aad0832.
[58] F.J. García-Mateos, R. Berenguer, M.J. Valero-Romero, J. Rodríguez-Mirasol, T. Cordero, Phosphorus functionalization for the rapid preparation of highly nanoporous submicron-diameter carbon fibers by electrospinning of lignin solutions, J. Mater. Chem. A Mater. 6 (2018) 1219–1233, https://doi.org/10.1039/C7TA08788H.
[59] S. Kubo, J.F. Kadla, Lignin-based carbon fibers: effect of synthetic polymer blending on fiber properties, J. Polym. Environ. 13 (2005) 97–105, https://doi.org/10.1007/S10924-005-2941-0.
[60] J.F. Kadla, S. Kubo, R.A. Venditti, R.D. Gilbert, A.L. Compere, W. Griffith, Lignin-based carbon fibers for composite fiber applications, Carbon 40 (2002) 2913–2920, https://doi.org/10.1016/S0008-6223(02)00248-8.
[61] X. Wang, W. Li, D. Xiong, D.Y. Petrovykh, L. Liu, Bifunctional nickel phosphide nanocatalysts supported on carbon fiber paper for highly efficient and stable overall water splitting, Adv. Funct. Mater. 26 (2016) 4067–4077, https://doi.org/10.1002/ADFM.201505509.
[62] M.J. Mostazo-López, R. Ruiz-Rosas, E. Morallón, D. Cazorla-Amorós, Generation of nitrogen functionalities on activated carbons by amidation reactions and Hofmann rearrangement: chemical and electrochemical characterization, Carbon 91 (2015), https://doi.org/10.1016/j.carbon.2015.04.089.
[63] P. Cabrera-Reyes, J. Palomo, F.J. García-Mateos, R. Ruiz-Rosas, J.M. Rosas, J. Rodríguez-Mirasol, T. Cordero, Sustainable carbon-based nickel catalysts for the steam reforming of model compounds of pyrolysis liquids, Fuel Process. Technol. 253 (2024) 108028, https://doi.org/10.1016/J.FUPROC.2023.108028.
[64] C.D. Jaimes-Paez, F.J. García-Mateos, R. Ruiz-Rosas, J. Rodríguez-Mirasol, T. Cordero, E. Morallón, D. Cazorla-Amorós, Sustainable synthesis of metal-doped lignin-derived electrospun carbon fibers for the development of ORR electrocatalysts, Nanomaterials 13 (2023) 2921, https://doi.org/10.3390/NANO13222921/S1.
[65] J. Chmiola, G. Yushin, Y. Gogotsi, C. Portet, P. Simon, P.L. Taberna, Anomalous increase in carbon at pore sizes less than 1 nanometer, Science 313 (2006) 1760–1763, https://doi.org/10.1126/science.1132195.
[66] L. Eliad, G. Salitra, A. Soffer, D. Aurbach, Ion sieving effects in the electrical double layer of porous carbon electrodes: estimating effective ion size in electrolytic solutions, J. Phys. Chem. B 105 (2001) 6880–6887, https://doi.org/10.1021/JP010086Y.
[67] M. Zirbes, S.R. Waldvogel, Electro-conversion as sustainable method for the fine chemical production from the biopolymer lignin, Curr. Opin. Green Sustainable Chem. 14 (2018) 19–25, https://doi.org/10.1016/J.COGSC.2018.05.001.
[68] L.F. Li, Y.F. Li, Z.P. Liu, Oxygen evolution activity on NiOOH catalysts: four-coordinated Ni cation as the active site and the hydroperoxide mechanism, ACS Catal. 10 (2020) 2581–2590, https://doi.org/10.1021/acscatal.9b04975.
[69] K. Juodkazis, J. Juodkazytė, R. Vilkauskaitė, V. Jasulaitienė, Nickel surface anodic oxidation and electrocatalysis of oxygen evolution, J. Solid State Electrochem. 12 (2008) 1469–1479, https://doi.org/10.1007/s10008-007-0484-0.
[70] M. Zirbes, D. Schmitt, N. Beiser, D. Pitton, T. Hoffmann, S.R. Waldvogel, Anodic degradation of lignin at active transition metal-based alloys and performance-enhanced anodes, Chemelectrochem 6 (2019) 155–161, https://doi.org/10.1002/CELC.201801218.
[71] N. Di Fidio, J.W. Timmermans, C. Antonetti, A.M. Raspolli Galletti, R.J. A. Gosselink, R.J.M. Bisselink, T.M. Slaghek, Electro-oxidative depolymerisation of technical lignin in water using platinum, nickel oxide hydroxide and graphite electrodes, New J. Chem. 45 (2021) 9647–9657, https://doi.org/10.1039/D1NJ01037A.
[72] Z. Fang, M.G. Flynn, J.E. Jackson, E.L. Hegg, Thio-assisted reductive electrolytic cleavage of lignin β-O-4 models and authentic lignin, Green Chem. 23 (2021) 412–421, https://doi.org/10.1039/D0GC03597A.
[73] Z. Fang, F. Li, M. Wang, F. Li, X. Wu, K. Fan, Q. Tang, L. Sun, P. Zhang, Selective electrocatalytic upgrading of lignin to aryl aldehydes and carboxylic acids over dodecyl sulfate-intercalated CoS nanocones, Appl. Catal., B 323 (2023) 122149, https://doi.org/10.1016/J.APCATB.2022.122149.
[74] Z. Danlu, Z. Xu, W. Sinong, X. Yan, D. Qiqi, Y. Fengxia, W. Peng, L. Chuanfu, L. Wu, Electrochemical oxidation of lignin model compounds over metal oxyhydroxides on nickel foam, Green Chem. 26 (2024) 7759–7768, https://doi.org/10.1039/D4GC02156H.
[75] Z. Ying, H. Sun, J. Cao, X. Zheng, B. Dou, G. Cui, Lignin oxidation reaction kinetics and its conversion into high-value chemicals over self-prepared electrode during lignin-assisted water electrolysis for hydrogen production, Renew. Energy 237 (2024) 121746, https://doi.org/10.1016/J.RENENE.2024.121746.
[76] K. Beliaeva, N. Grimaldos-Osorio, E. Ruiz-López, L. Burel, P. Vernoux, A. Caravaca, New insights into lignin electrolysis on nickel-based electrocatalysts: electrochemical performances before and after oxygen evolution, Int. J. Hydrogen Energy 46 (2021) 35752–35764, https://doi.org/10.1016/J.IJHYDENE.2021.01.224.
[77] J. Sun, J. Wang, Y. Jia, S. Zhuang, Y. Xie, X. Yin, Y. Zhang, R. Zhao, H. Tan, L. Wang, F. Song, H. Cui, Depolymerization of lignin model compounds by reactive oxygen species generated from peroxymonosulfate under mild conditions, Biomass Bioenergy 179 (2023) 106973, https://doi.org/10.1016/J.BIOMBIOE.2023.106973.
[78] J. Xue, D. Wang, X. Li, G. Li, Z. Wang, Y. Liu, X. Li, A tandem strategy of mild preoxidation-hydrogenolysis for efficient depolymerization of lignin, Mol. Catal. 549 (2023) 113529, https://doi.org/10.1016/J.MCAT.2023.113529.
[79] R. Rani, N. Kumar, B. Paul, Hydrogen peroxide assisted oxidative liquefaction of alkaline lignin over cobalt-nickel loaded zirconia catalysts, J. Energy Inst. 115 (2024) 101709, https://doi.org/10.1016/J.JOEI.2024.101709.
[80] S. Cotillas, J. Llanos, M.A. Rodrigo, P. Cañizares, Use of carbon felt cathodes for the electrochemical reclamation of urban treated wastewaters, Appl. Catal., B 162 (2015) 252–259, https://doi.org/10.1016/J.APCATB.2014.07.004.
[81] J.F. Pérez, C. Sáez, J. Llanos, P. Cañizares, C. López, M.A. Rodrigo, Improving the efficiency of carbon cloth for the electrogeneration of H_2O_2: role of polytetrafluoroethylene and carbon black loading, Ind. Eng. Chem. Res. 56 (2017) 12588–12595, https://doi.org/10.1021/acs.iecr.7b02563.
[82] D. Schmitt, C. Regenbrecht, M. Hartmer, F. Stecker, S.R. Waldvogel, Highly selective generation of vanillin by anodic degradation of lignin: a combined approach of electrochemistry and product isolation by adsorption, Beilstein J. Org. Chem. 11 (2015) 473–480, https://doi.org/10.3762/bjoc.11.53.
[83] J. Han, R. Lin, M. Salehi, A. Farzi, A. Carkner, K. Liu, O. Abou El-Oon, O. Ajao, A. Seifitokaldani, Kraft lignin electro-oxidation under ambient temperature and pressure, Energies 16 (2023) 8007, https://doi.org/10.3390/EN16248007/S1.
[84] R.S. Weber, K.K. Ramasamy, Electrochemical oxidation of lignin and waste plastic, ACS Omega 5 (2020) 27735–27740, https://doi.org/10.1021/acsomega.0c03989.
[85] K.K. Pandey, A study of chemical structure of soft and hardwood and wood polymers by FTIR spectroscopy, J. Appl. Polym. Sci. 71 (71) (1999) 1969–1975, https://doi.org/10.1002/(SICI)1097-4628(19990321, 12.
[86] F. Monteil-Rivera, M. Phuong, M. Ye, A. Halasz, J. Hawari, Isolation and characterization of herbaceous lignins for applications in biomaterials, Ind. Crops Prod. 41 (2013) 356–364, https://doi.org/10.1016/J.INDCROP.2012.04.049.
[87] J.J. Conde, S. González-Rodríguez, X. Chen, T.A. Lu-Chau, G. Eibes, A. Pizzi, M. T. Moreira, Electrochemical oxidation of lignin for the simultaneous production of bioadhesive precursors and value-added chemicals, Biomass Bioenergy 169 (2023) 106693, https://doi.org/10.1016/J.BIOMBIOE.2022.106693.